

InvertAvatar: Incremental GAN Inversion for Generalized Head Avatars

XIAOCHEN ZHAO*, Tsinghua University, China

JINGXIANG SUN*, Tsinghua University, China

LIZHEN WANG, Tsinghua University, China

JINLI SUO, Tsinghua University, China

YEBIN LIU†, Tsinghua University, China



Fig. 1. Given single or more source images, our method rapidly reconstructs photorealistic 3D facial avatars under one second, enabling precise control over full-head rotations and subtle expressions like lopsided grins and eye gazes.

While high fidelity and efficiency are central to the creation of digital head avatars, recent methods relying on 2D or 3D generative models often experience limitations such as shape distortion, expression inaccuracy, and identity flickering. Additionally, existing one-shot inversion techniques fail to fully leverage multiple input images for detailed feature extraction. We propose a novel framework, **Incremental 3D GAN Inversion**, that enhances avatar reconstruction performance using an algorithm designed to increase the fidelity from multiple frames, resulting in improved reconstruction quality proportional to frame count. Our method introduces a unique animatable 3D GAN prior with two crucial modifications for enhanced expression controllability alongside an innovative neural texture

encoder that categorizes texture feature spaces based on UV parameterization. Differentiating from traditional techniques, our architecture emphasizes pixel-aligned image-to-image translation, mitigating the need to learn correspondences between observation and canonical spaces. Furthermore, we incorporate ConvGRU-based recurrent networks for temporal data aggregation from multiple frames, boosting geometry and texture detail reconstruction. The proposed paradigm demonstrates state-of-the-art performance on one-shot and few-shot avatar animation tasks. Code will be available at <https://github.com/XChenZ/invertAvatar>.

CCS Concepts: • **Computing methodologies** → *Motion processing*; **Image-based rendering**.

Additional Key Words and Phrases: 3D head avatar, one-shot reconstruction, few-shot reconstruction, recurrent neural network, GAN inversion

ACM Reference Format:

XIAOCHEN ZHAO, JINGXIANG SUN, LIZHEN WANG, JINLI SUO, and YEBIN LIU. 2024. InvertAvatar: Incremental GAN Inversion for Generalized Head Avatars. In *Special Interest Group on Computer Graphics and Interactive Techniques Conference Conference Papers '24 (SIGGRAPH Conference Papers '24)*, July 27–August 1, 2024, Denver, CO, USA. ACM, New York, NY, USA, 15 pages. <https://doi.org/10.1145/3641519.3657478>

*Both authors contributed equally to the paper

† Corresponding authors

Permission to make digital or hard copies of part or all of this work for personal or classroom use is granted without fee provided that copies are not made or distributed for profit or commercial advantage and that copies bear this notice and the full citation on the first page. Copyrights for third-party components of this work must be honored. For all other uses, contact the owner/author(s).

SIGGRAPH Conference Papers '24, July 27–August 1, 2024, Denver, CO, USA

© 2024 Copyright held by the owner/author(s).

ACM ISBN 979-8-4007-0525-0/24/07.

<https://doi.org/10.1145/3641519.3657478>

1 INTRODUCTION

The creation of digital head avatars [Athar et al. 2022; Deng et al. 2020; Doukas et al. 2021; Gafni et al. 2021; Grassal et al. 2022; Ren et al. 2021; Wang et al. 2023; Zhang et al. 2022; Zheng et al. 2022, 2023] has long been a task of interest in the fields of computer vision and graphics. The ability to interactively generate photo-realistic head avatars opens up new possibilities in areas such as augmented/virtual reality (AR/VR), 3D telepresence, and video conferencing. The primary aims when developing a digital head avatar are two-fold: high fidelity and efficiency. High fidelity involves preserving intricate details from input images, reconstructing occluded facial regions (especially in profile views), and accurately modeling dynamic features such as facial expressions, while maintaining consistent identity throughout animation. Efficiency demands a model that can adapt to varied unseen identities and motions without additional optimization at the inference stage.

Recent literature showcases numerous attempts to create avatars from a single input image and perform animation with video frames. Several 2D generative models [Deng et al. 2020; Doukas et al. 2021; Ren et al. 2021; Wang et al. 2023] perform image animation by incorporating the 3D Morphable Face Models (3DMM) [Blanz and Vetter 1999] into the portrait synthesis. These 2D-based methods achieve photo-realism but suffer from shape distortion during large motion due to a lack of geometry constraints.

Towards better view consistency, many recent efforts [Bai et al. 2023; Ma et al. 2023] leverage 3D GAN prior and decouple motion and appearance in latent space with video data. The main drawback of this paradigm is that the motion and appearance are naturally entangled in 3D GAN which leads to expression inaccuracy and identity flickering during animation. The other line of works [Li et al. 2023a; Sun et al. 2023; Tang et al. 2023; Wu et al. 2022] directly learn a controllable 3D GAN from only 2D image collections, and perform GAN inversion to restore an avatar from one single image. The methods employing the controllable generative prior demonstrate efficiency, yet they are constrained by their dependency on a singular source image. A single image often falls short in fully representing the subject owing to factors such as occlusions and limited pose information. Utilizing diverse source images enriches appearance data, thereby diminishing the extent of hallucination required by an image generator. However, these one-shot inversion techniques do not directly enable the aggregation of partial observations across distinct frames to reconstruct more personalized details. Consequently, this represents a significant limitation to their capacity for detailed feature extraction.

In this paper, we address the challenge of enhancing avatar reconstruction performance when multiple input images are present. Our proposed algorithm is designed to elevate the fidelity of the recovered avatar both within and beyond the face region across multiple frames, with improvements in personal detail reconstruction scaling with the increase in frame count. To achieve this, we introduce a novel framework capable of efficient incremental 3D head avatar reconstruction, fusing multiple inputs without necessitating any additional optimization during inference from a sequence of monocular images.

Specifically, we utilize an animatable 3D GAN prior, incorporating two key modifications to enhance expression controllability’s efficiency and accuracy. Subsequently, we introduce an innovative neural texture encoder designed to categorize texture feature spaces in accordance with UV parameterization. This differentiates our approach from prevalent techniques that depend on networks to map an unposed image to a canonical tri-plane representation. Our proposed architecture emphasizes pixel-aligned image-to-image translation, which effectively eradicates the need for learning correspondences between observation and canonical spaces. This focus significantly improves its capacity for recovering fine details.

To accumulate temporal data from numerous frames, we further modify the one-shot inversion architecture to accommodate multiple inputs by leveraging ConvGRU-based [Ballas et al. 2015] recurrent networks. This unique recurrent mechanism allows a flexible number of inputs and autonomously determines which information should be retained or discarded within streaming frames, thereby bolstering geometry and texture detail reconstruction capabilities.

To summarize, the contributions of our approach are:

- We provide a new paradigm for efficient avatar reconstruction for streaming data based on a concept called incremental 3D GAN inversion. The paradigm supports one to multiple source images inputs and achieves state-of-the-art performance on one- and few-shot facial avatar animation tasks.
- We propose an innovative neural texture encoder alongside an animatable 3D GAN prior, allowing for the definition of a texture feature space on the UV parameterization which enhances the recovery of fine details by pixel-aligned nature.
- We incorporate recurrent networks for temporal aggregation from multiple input frames extracted from monocular video, enhancing the quality of avatar reconstruction by considering sequential data.

2 RELATED WORKS

2.1 3D GAN inversion

Building upon the achievements of 2D Generative Adversarial Network (GAN) inversion for image editing and manipulation [Alaluf et al. 2021; Dinh et al. 2022; Richardson et al. 2021; Tov et al. 2021; Wang et al. 2022b], current 3D GAN inversion methodologies [Ko et al. 2023; Lin et al. 2022; Sun et al. 2022] perform a projection of specific images onto multiple instances within the pre-trained StyleGAN2 latent space [Abdal et al. 2019; Karras et al. 2020]. While the global latent space enhances 3D-aware portrait editing abilities, it results in a trade-off between reconstruction accuracy and editability, thereby complicating the accurate reconstruction of input images. Consequently, contemporary 3D GAN inversion techniques necessitate an estimated camera pose and slight generator weight adjustment [Feng et al. 2022; Roich et al. 2021; Xie et al. 2023] during testing to reconstruct out-of-domain input images accurately. In contrast to latent code inversion or tedious generator fine-tuning, recent efforts have shifted towards directly applying 3D GAN inversion on a triplane architecture for 3D GANs. For instance, TriPlaneNet [Bhattarai et al. 2023] presents a triplane encoder while

Live3DPortrait [Trevithick et al. 2023] integrates a Vision Transformer architecture into the triplane encoder, both showing substantial enhancements in robustness and 3D inversion quality for out-of-domain images. Furthermore, Control3Diff [Gu et al. 2023] suggests a diffusion-based tri-plane encoder that demonstrates multimodal control capabilities.

2.2 2D Facial animation

Leveraging the benefits of 3DMM, 2D facial animation tasks [Gecer et al. 2019; Thies et al. 2016] are able to accurately and continuously model facial part deformations. However, these methods tend to lack fine-grained facial details, and grapple with representing non-facial areas that are beyond the scope of 3DMM, such as hair, teeth, eyes, and body. To compensate for these limitations and generate more realistic facial details, subsequent research [Deng et al. 2020; Doukas et al. 2021; Fried et al. 2019; Gecer et al. 2018; Kim et al. 2018; Ren et al. 2021; Tewari et al. 2020; Thies et al. 2019; Wang et al. 2023; Xu et al. 2020] has applied learned techniques atop 3DMM renderings. Getting rid of 3DMM, some methods [Burkov et al. 2020; Drobyshev et al. 2022; Liang et al. 2022; Wang et al. 2021b] are trained on the large-scale face video datasets containing rich identities and expressions, thus can be generalized to unseen motion and identity given just a single input image. While these 2D-based approaches have successfully facilitated efficient and photorealistic animation, they do not model 3D geometry and hence fail to maintain stringent 3D consistency during significant head pose alterations.

2.3 Neural 3D head avatars

For strict 3D consistency, recent efforts [Athar et al. 2022; Chen et al. 2024; Gafni et al. 2021; Grassal et al. 2022; Xu et al. 2024, 2023b; Zhang et al. 2022; Zhao et al. 2023; Zheng et al. 2022] incorporate 3DMM into implicit representations [Kanazawa et al. 2018; Kerbl et al. 2023; Mildenhall et al. 2020; Peng et al. 2020; Sitzmann et al. 2019] to achieve view-consistent facial animation. Although these methods demonstrate realistic reconstruction results, they inefficiently learn separate networks for different identities and require thousands of frames from a specific individual for training. Another line of works [Bai et al. 2023; Li et al. 2023b,a; Ma et al. 2023; Sun et al. 2023; Xu et al. 2023a; Yu et al. 2023] focus on reconstructing 3D portraits in one-shot or few-shot manner incorporating 3D GAN prior or training in a generative manner. Next3D [Sun et al. 2023] learns a controllable 3D head avatar from random noise and reconstructs an avatar by PTI inversion. [Li et al. 2023a] proposes to encode input images into a canonical branch for coarse geometry and texture, and introduces an additional appearance branch that captures personal details and an expression branch that modifies the reconstruction to the desired expression. These methods show efficient promising one-shot reconstruction but none of them are architected to accommodate the utilization of multiple source images as input. Contrastingly, our proposed framework is designed to leverage the complementary information inherent in multiple input images, thereby facilitating superior reconstruction quality.

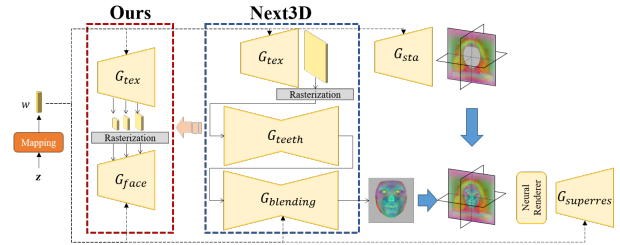


Fig. 2. The architecture review of Next3D, along with the visualization of the modifications in our adopted 3D generative model.

3 METHOD

Our method innovatively harnesses the prior knowledge embedded in an animatable 3D generative model, integrating it with an incremental inversion architecture to enable rapid and high-fidelity 3D avatar reconstruction. Utilizing either a single source image or a short sequence of dynamic frames from a source video, our system is capable of reconstructing a 3D facial avatar, which is readily animatable through a 3D Morphable Face Model (3DMM) [Wang et al. 2022a]. In Sec. 3.2, we introduce our compact yet highly expressive animatable GAN, which provides a strong 3D prior. Sec. 3.3 details our one-shot learning-based avatar reconstruction method, intricately designed to capitalize on the aforementioned GAN prior. Conclusively, in Section 3.4, we describe the employment of RNN-based temporal aggregation networks, which are instrumental in enhancing the shape and appearance precision of the reconstructed avatar by harnessing temporal data.

3.1 Preliminary: Next3D

Our chosen framework for animatable 3D GAN is Next3D [Sun et al. 2023], which currently stands as the SOTA in generating high-quality, 3D consistent facial avatars from unstructured 2D images. The innovation within Next3D lies in its proposed 3D representation, termed *Generative Texture-Rasterized Tri-planes*. Illustrated in Fig. 2, given a randomly sampled latent code z , the mapping network maps z to an intermediate latent code w . This intermediate latent code modulates a StyleGAN generator to synthesize Generative Neural Textures atop parametric mesh templates. Subsequently, these are projected onto three orthogonally oriented feature planes via rasterization of a conditional facial 3DMM, thus establishing a tri-plane feature schema for volume rendering and 2D super-resolution ($G_{superres}$). This dual approach combines the nuanced expression control afforded by mesh-guided explicit deformation with the adaptive prowess of implicit volumetric representation. For more details please refer to [Sun et al. 2023].

3.2 Compact and Expressive Animatable 3D GAN

Drawing from Next3D for our 3D facial avatar generator, we make the following improvements for our avatar reconstruction task. First, since 3DMM does not contain the inner mouth area, Next3D supplements and reintegrates the inner mouth features by two additional UNets, which leads to additional complexity and meory burden. To improve this, as shown in Fig. 2, we replace the two UNets with

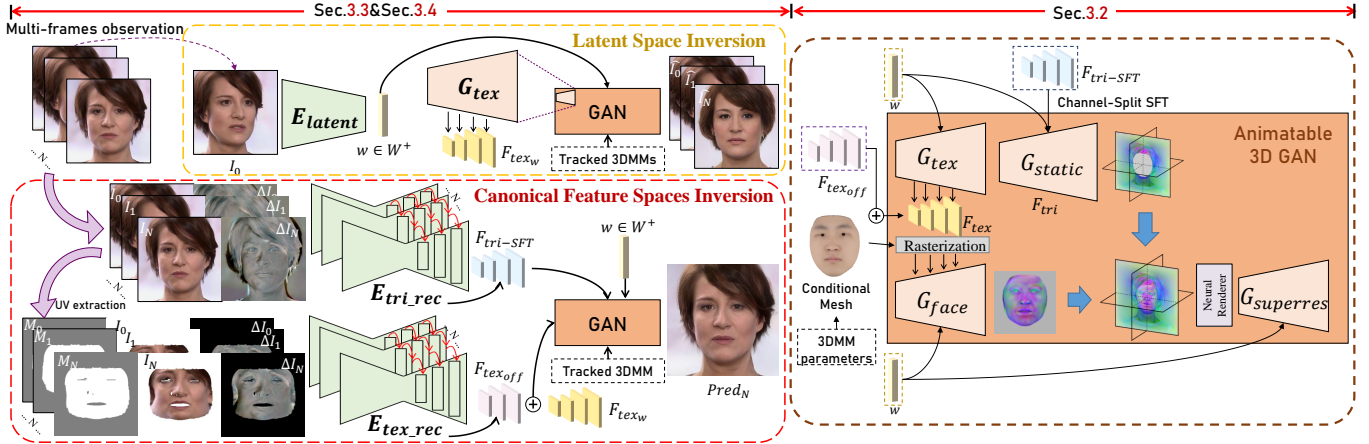


Fig. 3. The left part illustrates our two-stage avatar reconstruction pipeline. The coarse stage “Latent Space Inversion” (Sec.3.3) inverts the first frame in the GAN prior’s W^+ latent space with E_{latent} , forming an initial avatar. The fine stage performs offset prediction in canonical feature spaces (Sec.3.4) and we specifically design recurrent networks E_{tex_rec} and E_{tri_rec} to aggregate temporal information, incrementally refining a high-fidelity avatar (Sec.3.4). The architecture of our advanced animatable 3D generative model is depicted in the right box.

a single generator G_{face} by conditioning G_{face} with the multi-scale rasterized neural texture feature maps, which allows the inner mouth features to be gradually generated through multiple convolutional layers. Consequently, our more memory-efficient model design allows for larger neural rendering resolution of 128^2 .

Besides, we practically notice that the misalignment between conditional 3DMM and 2D image expressions can weaken their correlation during adversarial training, impeding the correct deformation of generated images. To rectify this, we employ Faceverse [Wang et al. 2022a], a parametric model with more expression bases, to accurately fit subtle expression changes in 2D images. During training, we also supply the discriminator with the tracked landmarks map to bolster the consistency between synthesized images and the conditional mesh.

In the subsequent inversion and animation phases, we will initially fit Faceverse to the source portrait image or images of a person, capturing their expressions and head poses. Next, GAN inversion will be applied to reconstruct the corresponding head character. Finally, by changing the input expression parameters of FaceVerse, we gain the ability to animate the inverted avatar.

3.3 One-shot Avatar Reconstruction

To extract maximum personal information from a single image with the reconstructed avatar, we introduce an effective one-shot 3D GAN inversion framework. This framework utilizes a coarse-to-fine inversion architecture that carries out inversions in the latent and feature spaces of our animatable generative model separately. Due to the disentangled nature of the dynamic face and static head features, we divide the feature space into two specific canonical spaces: F_{tex} defined by G_{tex} (the canonical texture space), and F_{tri} defined by G_{static} (the canonical tri-plane space). The ultimate goal then becomes learning the mapping from the input portrait image to the facial avatar represented in these latent and canonical feature spaces.

In the first stage, we introduce a latent encoder E_{latent} to project the image to the W^+ latent space of the pretrained GAN. Specifically, given a source image I , we embed an inverted latent code $\hat{w} = E_{latent}(I)$ and initially generate a coarse facial avatar, represented by canonical features $F_{tex_w} = G_{tex}(\hat{w})$ and $F_{tri_w} = G_{static}(\hat{w})$. With the estimated pose and expression of the source image I , we can synthesize the fake image $\hat{I} = R(G_{face}(F_{tex_w}), F_{tri_w})$, where R is the rendering block.

In the second stage, with the aim to offset the information loss instigated by E_{latent} , we formulate two separate image encoders E_{tex} and E_{tri} . These are specifically designed to refine the feature maps in each of the two canonical spaces independently. Different from existing methods that rely on networks to map a posed image to the canonical tri-plane representation, benefiting from the neural texture architecture of our GAN prior, the face appearance represented by texture feature space is explicitly defined on the UV parameterization. Hence we design a U-Net network E_{tex} to translate the observation to the canonical texture feature space in the UV domain, as shown in Fig. 3¹. Such a pixel-aligned image-to-image translation architecture helps eliminate the learning burden of correspondences between observation space and canonical space, making it concentrate on recovering fine details, as demonstrated in Sec. 4.3.2. Specifically, the input of the E_{tex} contains three maps, the source image I and the residual map $\Delta I = I - \hat{I}$ that are projected to the UV plane, and a mask indicating the visibility region of the face. E_{tex} outputs multi-resolution feature offsets F_{tex_off} to compensate for the texture features F_{tex_w} obtained in the first stage.

As for the static tri-plane features, we introduce an image-to-plane encoder E_{tri} to predict multi-scale feature maps. Specifically, the multi-resolution features F_{tri_SFT} output by E_{tri} are used to

¹ E_{tex_rec} in Fig. 3 refers to the encoder E_{tex} equipped with a recurrent decoder. We describe it in Sec. 3.4 in detail.

spatially modulate G_{static} with the Channel-Split SFT² layer [Wang et al. 2021a] in a coarse-to-fine manner.

The training for all image encoders can also be divided into two stages. Firstly, we only train E_{latent} , with the loss terms following [Richardson et al. 2021; Tov et al. 2021]. Secondly, we simultaneously train E_{tex} and E_{tri} . Referring to Live 3D Portrait [Trevithick et al. 2023], our training set includes the synthetic data and we supervise the training with many intermediate feature maps, as well as an adversarial loss to generate photo-realistic results. Please refer to our supplemental material for more details.

3.4 Incremental GAN inversion

While the aforementioned GAN encoder effectively facilitates high-quality one-shot avatar reconstruction, a solitary image lacks sufficient pose and expression information to fully portray the shape and appearance. Therefore, we propose an approach termed *Incremental GAN Inversion*: incrementally enhances the quality of GAN inversion while concurrently integrating temporal information.

We transition from a one-shot to a multi-frame inversion structure using temporal aggregation networks E_{tex_rec} and E_{tri_rec} equipped with recurrent decoders. Given an input video clip $I^N = \{I_t\}_0^N$, we aim at fusing the information of all frames to generate canonical representation F_{tex} and F_{tri} . First, the first frame is input to the E_{latent} for $W+$ space latent code w and initial canonical features $F_{tex,w}$ and $F_{tri,w}$. According to the poses and expressions of the input sequence, we synthesize a fake image sequence and calculate the residual map for each frame $\Delta I_t = I_t - \hat{I}_t$. We sequentially input the observation and residual of each frame into the network E_{tex_rec} and E_{tri_rec} respectively on the UV domain and the picture domain.

Performing in a seq2one fashion, the recurrent decoders of E_{tex_rec} and E_{tri_tex} merge frame-wise feature maps in the temporal domain to predict one $F_{tri-SFT}$ and F_{tex_off} . Specifically, the recurrent decoder adopts ConvGRU [Ballas et al. 2015] at each scale to aggregate temporal information, which is defined as:

$$\begin{aligned} z_t, r_t &= \sigma(\text{Conv}(f_t, h_{t-1})) \\ o_t &= \tanh(\text{Conv}(f_t, r_t * h_{t-1})) \\ h_t &= z_t * h_{t-1} + (1 - z_t) * o_t \end{aligned} \quad (1)$$

where operator $*$ denotes element-wise product. For each ConvGRU block, the feature map of one frame f_t is input to calculate the update weights map z_t and reset weights map r_t , to merge the current frame’s information into hidden state h_t . With the initial recurrent state h_0 all zero tensor, after inputting all frames in turn, the final fully updated hidden state serves as the output.

Contrary to systems employing straightforward feed forwarding of multiple frames as auxiliary inputs, our recurrent mechanism accommodates a flexible number of inputs. It intelligently learns the information to keep or discard from streaming data, thereby circumventing the constraints of fixed-size input windows and interval-based updates.

²Channel-Split Spatial Feature Transform is a layer tailored for the StyleGAN2 backbone to perform spatial modulation while preserving the generative prior.



Fig. 4. Compare our animatable 3D generative model with Next3D [Sun et al. 2023]. We extract frames from a driving video clip and use the estimated facial model parameters to animate sampled random virtual avatars. Please zoom in and also refer to our video for more clear comparisons.

Table 1. Quantitative comparison with Next3D on image synthesis quality, animation accuracy, identity preservation and memory consumption.

	FID↓	AKD↓	CSIM↑	Params
Ours	4.1	0.057	0.853	84.21M
Next3D	3.9	0.248	0.841	164.81M

4 EXPERIMENTS

4.1 Experiment Setting

Baseline methods. Firstly, we compare the utilized animatable 3D GAN prior with Next3D [Sun et al. 2023]. Then, we mainly compare our method with image-driven-based generalized head avatar reenactment methods, including a 2D face reenactment method [Yin et al. 2022] and two 3D avatar synthesis methods [Khakhulin et al. 2022; Ma et al. 2023]. We also compare with an optimization-based baseline Next3D-PTI, which incorporates an animatable 3D GAN [Sun et al. 2023] and pivotal tuning inversion [Roich et al. 2021]. We do not make comparisons with person-specific head avatar methods, since these multi-shot methods cannot generalize to different identities.

Evaluation Metrics. We evaluate generation, reconstruction and reenactment quality using Frechet Inception Distance (FID) [Heusel et al. 2017], peak signal-to-noise ratio (PSNR), Learned Perceptual Image Patch Similarity (LPIPS) [Zhang et al. 2018] for synthetic quality, cosine similarity (CSIM) [Deng et al. 2019] for identity preservation, and average keypoint distance (AKD) using a SOTA off-the-shelf facial landmarks detector³ for reenactment quality.

³<https://github.com/google/mediapipe>

Table 2. Quantitative Evaluation for one-shot avatar reconstruction and animation.

Method	Same-ID on HDTF					Cross-ID on HDTF		Cross-ID on CelebA	
	PSNR \uparrow	L1 \downarrow	LPIPS \downarrow	CSIM \uparrow	AKD \downarrow	CSIM \uparrow	AKD \downarrow	CSIM \uparrow	AKD \downarrow
Ours	23.27	0.029	0.111	0.873	0.018	0.759	0.041	0.755	0.069
OTAvatar	22.85	0.035	0.133	0.794	0.136	0.669	0.420	0.569	2.050
Next3D-PTI	22.05	0.038	0.128	0.850	0.312	0.651	0.577	0.648	0.788
StyleHEAT	22.32	0.036	0.130	0.827	0.109	0.710	0.216	0.604	0.348
ROME	22.91	0.034	0.127	0.832	0.120	0.722	0.239	0.682	0.299

Table 3. Quantitative Evaluation on VFHQ-Test using multiple source images.

	2 source frames					4 source frames				
	PSNR \uparrow	LPIPS \downarrow	AKD \downarrow	CSIM \uparrow	Time(s)	PSNR \uparrow	LPIPS \downarrow	AKD \downarrow	CSIM \uparrow	Time(s)
Ours	23.39	0.170	0.024	0.867	0.20	23.58	0.162	0.022	0.873	0.32
OTAvatar	17.39	0.281	0.696	0.736	50	17.76	0.276	0.614	0.721	100
Ours-OS	22.40	0.202	0.029	0.846	0.36	22.78	0.202	0.026	0.839	0.71
Next3D-PTI	20.23	0.199	0.637	0.821	150	20.74	0.1771	0.287	0.845	150

4.2 Comparisons

4.2.1 Animatable 3D GAN prior. To validate the superiority of our compact and expressive animatable 3D GAN, we compare our generative model with Next3D. Fig. 4 and Tab. 1 demonstrate qualitative and quantitative results. We measure image quality with FID between the entire VFHQ dataset and 50k generated images using randomly sampled latent codes, camera poses and estimated facial model parameters. Then we randomly sample 100 identities and animate each with randomly sampled 100 images from VFHQ, synthesizing 10000 images. AKD is calculated between the driving images and the animated generated ones, and CSIM is calculated for each identity. The comparison proves that, with roughly half the number of parameters, our generative model achieves the similar synthesis quality as Next3D and significantly improves animation accuracy. In the **supplemental video**, the video animation results present that Next3D suffers from shaking facial appearance and texture sticking artifacts, while our method achieves better temporal- and view-consistency.

4.2.2 One-shot Avatar Reconstruction. We evaluate same-identity and cross-identity reenactment using various methods. For self-reenactment, the first frame of HDTF test videos served as the source, with the next 500 frames as the driving video. In cross-identity cases, the first 200 frames of one HDTF clip compose the driving video, and the first frame of other videos as source images. Besides, following [Yin et al. 2022], We also transfer motions from videos to CelebA-HQ monocular images [Karras et al. 2018], using test videos from HDTF and VFHQ, creating 100,000 synthesized images from 1000 CelebA-HQ images and 25 video clips⁴. Without ground truth for cross-reenactment, we relied on CSIM and AKD metrics for evaluation.

Tab. 2 presents quantitative evaluations on the HDTF and CelebA-HQ datasets, while Fig. 8 showcases the qualitative results of cross-identity reenactment on the CelebA-HQ dataset. Our method shows

⁴In addition to 19 videos from the testing split of HDTF, we also select 6 videos with rich expression changes from VFHQ as supplements.

superior generalization on these unseen datasets, surpassing others in identity preservation, appearance recovery, and expression control. It outperforms baselines in capturing fine details such as hair strands and earrings. Additionally, it also excels in expression transfer, offering precise control over nuanced expressions like asymmetrical mouth movements and eye gazes. In comparison, ROME [Khakhulin et al. 2022] fails to capture high-frequency details, StyleHeat [Yin et al. 2022] struggles with inner mouth synthesis, and OTAvatar [Ma et al. 2023] is unable to generate photo-realistic facial avatars with compact latent vector encoding. Although Next3D-PTI can reconstruct avatars with test-time optimization, it falls short in precise expression control.

4.2.3 Few-shot Avatar Reconstruction. Without readily available benchmarks for few-shot avatar reconstruction, we adapt one-shot methods, both our method and OTAvatar [Ma et al. 2023], to accommodate multiple source images. This adaptation involves reconstructing canonical features from each source image, followed by averaging these features to derive a canonical space representation. Specifically, for OTAvatar, we compute the mean identity latent code. For our one-shot method, we averaged the feature maps F_{tex} and F_{tri} in both two canonical spaces.

Due to the diverse expressions and poses in VFHQ [Xie et al. 2022], we evaluate using a test dataset of 100 VFHQ videos, each with 300 frames, excluding training set subjects. We sample input frames evenly from the initial 200 frames and use the last 100 frames for performance evaluation.

Tab. 3 and Fig. 9 display the results obtained with varying numbers of input frames. Our incremental GAN inversion framework, in comparison to the one-shot inversion using only the first frame, adeptly integrates multi-frame data to fill in information gaps present in a single image, thus enhancing the geometry and texture details. For example, this is evident in the improved depiction of hair shape (row 1, Fig. 9), pupil color (row 2), and teeth refinement (row 3). Adapted one-shot methods, despite warping features from each source image to the canonical space, suffer from the misalignment

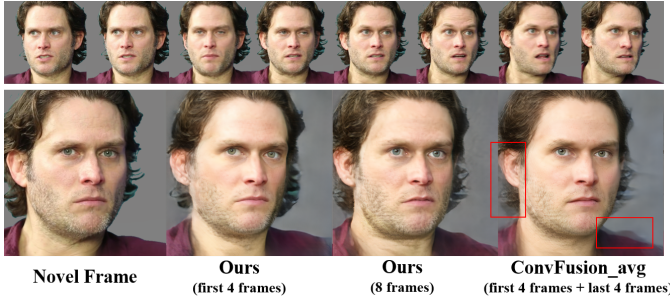


Fig. 5. With a continuous input video stream, our method incrementally refines facial shape and texture details, in contrast to the fixed-window baseline “ConvFusion_avg”, which tends to produce blurry outcomes.

of these inverted features, leading to blurry and inaccurate outputs. Our approach mitigates these issues, thanks to our RNN-based temporal aggregation network’s effectiveness in merging sequential features, which is critical for achieving realistic detail recovery, as seen in the hair strands in Fig. 1.

For efficiency, OTAvatar[Ma et al. 2023] and Next3D-PTI require lengthy optimization for novel identities. In contrast, our learning-based solution achieves rapid avatar reconstruction within one second, with the time cost increasing only marginally with the number of input frames.

4.3 Ablation Studies

4.3.1 Recurrent mechanism for temporal aggregation. To evaluate our recurrent mechanism, we establish a fixed-window baseline termed “ConvFusion”, which replaces each GRU block with a convolutional block to compress temporal features. Due to its fixed input capacity, “ConvFusion” averages the inverted canonical features when handling longer sequences.

Fig. 5 demonstrates the use of an 8-frame video clip to mimic an online stream. Our method shows incremental improvements in the reconstructed shape and appearance with the increase in frames. In contrast, “ConvFusion” lacks the ability to discern which information to retain or discard, and a simple averaging strategy results in a blurred feature space and inferior rendering results.

A similar pattern emerges in Fig. 6, where we simulate processing offline video sequences, assessing performance against the number of input frames. On the VFHQ-test, with denser sampling in the first 200-frame sequence, the error of “ConvFusion” initially decreases but then increases after the frame count exceeds its fixed-window size. Conversely, our recurrent framework’s performance improves incrementally with additional frames and then remains stable.

4.3.2 Encoder design for canonical space inversion .

Remove the second stage inversion. We set a baseline only utilizing E_{latent} . As shown in Fig. 7 and Tab. 4, without both E_{tex} and E_{tri} , the reconstructed portrait cannot recover the identity.

Prediction of tri-plane SFT parameters. We introduce a baseline approach that utilizes E_{tri} to directly predict feature offsets. As

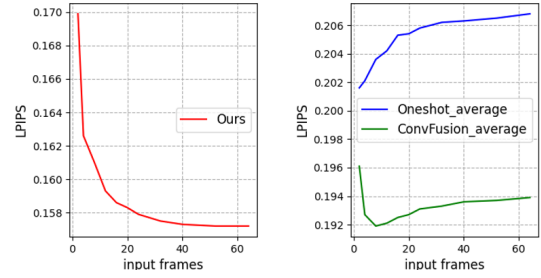


Fig. 6. LPIPS over the number of input frames on VFHQ-test. With longer sequences, our method shows improving and converging metrics, affirming its proficiency in long-term temporal aggregation, unlike fixed-window baselines that degrade as source image count consistently increases.

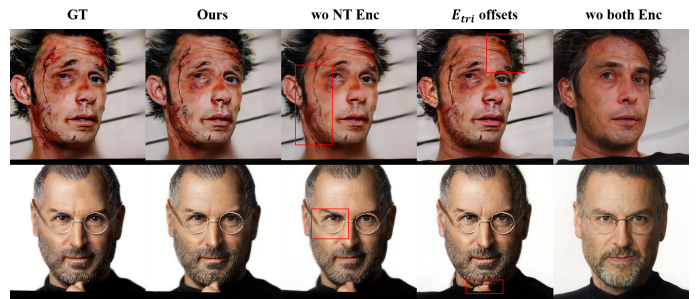


Fig. 7. Qualitative ablation study results on the encoder design for canonical space inversion. Zoom in for the best view.

Table 4. Ablation studies on CelebA-HQ for portrait reconstruction, to validate the effectiveness of our encoder design. We sample 1000 images to calculate metrics.

	LPIPS↓	PSNR↑	CSIM↑	FID↓
Ours	0.180	25.34	0.933	23.25
wo both Enc	0.393	17.67	0.809	26.42
wo NT Enc	0.201	24.35	0.910	28.23
E_{tri} offsets	0.244	21.97	0.889	34.36

illustrated in Fig. 7 and Tab. 4, our approach of predicting SFT parameters for modulating G_{sta} lessens the impact of the initial coarse facial avatar, thereby reducing artifacts and improving fidelity.

Neural Texture Encoder. We set a baseline with posed images as inputs to E_{tex} . As shown in Fig. 7 and Tab. 4, our neural texture encoder, designed to prioritize pixel-aligned image-to-image translation on the UV domain, is vital for faithful facial detail recovery.

5 DISCUSSION AND CONCLUSION

Limitation. Dependent on a parametric model to control facial expressions, our method is error-prone to tracking errors and struggles with extreme expressions beyond the model’s capability, like frowning and sticking tongue out. Additionally, synthesizing stable, clear dynamic lower teeth remains challenging. Future advancements

in more robust facial models capable of tracking these aspects are likely to enhance the performance.

Potential Social Impact. Considering our method can reconstruct a vivid personalized head character using a single image in less than one second, it may be used for generating “deepfakes”, which should be addressed carefully before deploying the technology.

Conclusion. We present *Incremental 3D GAN Inversion*, a feedforward pipeline for generalized 3D head avatar creation, supporting one or multiple image inputs. We employ an animatable 3D GAN prior and a novel UV-aligned neural texture encoder for detail recovery and ConvGRU-based recurrent networks for effective temporal fusing of streaming data. Experiments have demonstrated our method outperforms the state-of-the-art approaches in both one-shot and few-shot avatar animation tasks. We believe our method with a flexible number of input frames will make progress for the GAN inversion methods.

ACKNOWLEDGMENTS

This paper is supported by National Key R&D Program of China (2022YFF0902200), the NSFC project No.62125107.

REFERENCES

- Rameen Abdal, Yipeng Qin, and Peter Wonka. 2019. Image2StyleGAN: How to Embed Images Into the StyleGAN Latent Space?. In *Int. Conf. Comput. Vis.*
- Yuval Alaluf, Or Patashnik, and Daniel Cohen-Or. 2021. ReStyle: A Residual-Based StyleGAN Encoder via Iterative Refinement. In *Int. Conf. Comput. Vis.*
- ShahRukh Athar, Zexiang Xu, Kalyan Sunkavalli, Eli Shechtman, and Zhixin Shu. 2022. RigNeRF: Fully Controllable Neural 3D Portraits. In *IEEE Conf. Comput. Vis. Pattern Recog.*
- Yunpeng Bai, Yanbo Fan, Xuan Wang, Yong Zhang, Jingxiang Sun, Chun Yuan, and Ying Shan. 2023. High-fidelity Facial Avatar Reconstruction from Monocular Video with Generative Priors. In *Proceedings of the IEEE/CVF Conference on Computer Vision and Pattern Recognition*. 4541–4551.
- Nicolas Ballas, Li Yao, Chris Pal, and Aaron Courville. 2015. Delving deeper into convolutional networks for learning video representations. *arXiv preprint arXiv:1511.06432* (2015).
- Ananta R Bhattarai, Matthias Nießner, and Artem Sevastopolsky. 2023. TriPlaneNet: An Encoder for EG3D Inversion. *arXiv preprint arXiv:2303.13497* (2023).
- Volker Blanz and Thomas Vetter. 1999. A Morphable Model for the Synthesis of 3D Faces. In *Proceedings of the 26th Annual Conference on Computer Graphics and Interactive Techniques (SIGGRAPH '99)*. ACM Press/Addison-Wesley Publishing Co., USA, 187–194. <https://doi.org/10.1145/311535.311556>
- Egor Burkov, Igor Pasechnik, Artur Grigorev, and Victor Lempitsky. 2020. Neural head reenactment with latent pose descriptors. In *Proceedings of the IEEE/CVF conference on computer vision and pattern recognition*. 13786–13795.
- Eric R. Chan, Connor Z. Lin, Matthew A. Chan, Koki Nagano, Boxiao Pan, Shalini De Mello, Orazio Gallo, Leonidas Guibas, Jonathan Tremblay, Sameh Khamis, Tero Karras, and Gordon Wetzstein. 2022. Efficient Geometry-aware 3D Generative Adversarial Networks. In *IEEE Conf. Comput. Vis. Pattern Recog.*
- Yufan Chen, Lizhen Wang, Qijing Li, Hongjiang Xiao, Shengping Zhang, Hongxun Yao, and Yebin Liu. 2024. Monogaussianavatar: Monocular gaussian point-based head avatar. In *ACM SIGGRAPH 2024 Conference Proceedings*.
- Jiankang Deng, Jia Guo, Xue Niannan, and Stefanos Zafeiriou. 2019. ArcFace: Additive Angular Margin Loss for Deep Face Recognition. In *IEEE Conf. Comput. Vis. Pattern Recog.*
- Yu Deng, Jiaolong Yang, Dong Chen, Fang Wen, and Tong Xin. 2020. Disentangled and Controllable Face Image Generation via 3D Imitative-Contrastive Learning. In *Proceedings of the IEEE Conference on Computer Vision and Pattern Recognition (CVPR)*.
- Tan M. Dinh, Anh Tuan Tran, Rang Nguyen, and Binh-Son Hua. 2022. HyperInverter: Improving StyleGAN Inversion via Hypernetwork. In *IEEE Conf. Comput. Vis. Pattern Recog.*
- Michail Christos Doukas, Stefanos Zafeiriou, and Viktoriia Sharmanska. 2021. Headgan: One-shot neural head synthesis and editing. In *Proceedings of the IEEE/CVF International Conference on Computer Vision*. 14398–14407.
- Nikita Drobyshev, Jency Chelishve, Taras Khakhulin, Aleksei Ivakhnenko, Victor Lempitsky, and Egor Zakharov. 2022. Megaportraits: One-shot megapixel neural head avatars. In *Proceedings of the 30th ACM International Conference on Multimedia*. 2663–2671.
- Qianli Feng, Viraj Shah, Raghudeep Gadde, Pietro Perona, and Aleix Martinez. 2022. Near perfect gan inversion. *arXiv preprint arXiv:2202.11833* (2022).
- Ohad Fried, Ayush Tewari, Michael Zollhöfer, Adam Finkelstein, Eli Shechtman, Dan B Goldman, Kyle Genova, Zeyu Jin, Christian Theobalt, and Maneesh Agrawala. 2019. Text-based editing of talking-head video. *ACM Transactions on Graphics (TOG)* 38, 4 (2019), 1–14.
- Guy Gafni, Justus Thies, Michael Zollhofer, and Matthias Nießner. 2021. Dynamic neural radiance fields for monocular 4d facial avatar reconstruction. In *Proceedings of the IEEE/CVF Conference on Computer Vision and Pattern Recognition*. 8649–8658.
- Baris Geceer, Binod Bhattarai, Josef Kittler, and Tae-Kyun Kim. 2018. Semi-supervised adversarial learning to generate photorealistic face images of new identities from 3d morphable model. In *Proceedings of the European conference on computer vision (ECCV)*. 217–234.
- Baris Geceer, Stylianos Ploumpis, Irene Kotsia, and Stefanos Zafeiriou. 2019. Ganfit: Generative adversarial network fitting for high fidelity 3d face reconstruction. In *Proceedings of the IEEE/CVF conference on computer vision and pattern recognition*. 1155–1164.
- Philip-William Grassal, Malte Prinzler, Titus Leistner, Carsten Rother, Matthias Nießner, and Justus Thies. 2022. Neural head avatars from monocular RGB videos. In *Proceedings of the IEEE/CVF Conference on Computer Vision and Pattern Recognition*. 18653–18664.
- Jiatao Gu, Qingzhe Gao, Shuangfei Zhai, Baoquan Chen, Lingjie Liu, and Josh Susskind. 2023. Learning Controllable 3D Diffusion Models from Single-view Images. *arXiv preprint arXiv:2304.06700* (2023).
- Martin Heusel, Hubert Ramsauer, Thomas Unterthiner, Bernhard Nessler, Günter Klambauer, and Sepp Hochreiter. 2017. GANs Trained by a Two Time-Scale Update Rule Converge to a Nash Equilibrium.
- Angjoo Kanazawa, Shubham Tulsiani, Alexei A. Efros, and Jitendra Malik. 2018. Learning Category-Specific Mesh Reconstruction from Image Collections. In *Eur. Conf. Comput. Vis.*
- Tero Karras, Timo Aila, Samuli Laine, and Jaakko Lehtinen. 2018. Progressive Growing of GANs for Improved Quality, Stability, and Variation. In *Int. Conf. Learn. Represent.*
- Tero Karras, Samuli Laine, Miika Aittala, Janne Hellsten, Jaakko Lehtinen, and Timo Aila. 2020. Analyzing and Improving the Image Quality of StyleGAN. In *IEEE Conf. Comput. Vis. Pattern Recog.*
- Bernhard Kerbl, Georgios Kopanas, Thomas Leimkühler, and George Drettakis. 2023. 3d gaussian splatting for real-time radiance field rendering. *ACM Transactions on Graphics* 42, 4 (2023), 1–14.
- Taras Khakhulin, Vanessa Sklyarova, Victor Lempitsky, and Egor Zakharov. 2022. Realistic One-shot Mesh-based Head Avatars. In *Eur. Conf. Comput. Vis.*
- Hyeonwoo Kim, Pablo Garrido, Ayush Tewari, Weipeng Xu, Justus Thies, Matthias Niessner, Patrick Pérez, Christian Richardt, Michael Zollhöfer, and Christian Theobalt. 2018. Deep video portraits. *ACM Transactions on Graphics (TOG)* 37, 4 (2018), 1–14.
- Jaehoon Ko, Kysun Cho, Daewon Choi, Kwangrok Ryoo, and Seungryong Kim. 2023. 3D GAN Inversion with Pose Optimization. In *WACV*.
- Weichuang Li, Longhao Zhang, Dong Wang, Bin Zhao, Zhigang Wang, Mulin Chen, Bang Zhang, Zhongjian Wang, Liefeng Bo, and Xuelong Li. 2023b. One-Shot High-Fidelity Talking-Head Synthesis with Deformable Neural Radiance Field. In *Proceedings of the IEEE/CVF Conference on Computer Vision and Pattern Recognition*. 17969–17978.
- Xueting Li, Shalini De Mello, Sifei Liu, Koki Nagano, Umar Iqbal, and Jan Kautz. 2023a. Generalizable One-shot Neural Head Avatar. *arXiv preprint arXiv:2306.08768* (2023).
- Borong Liang, Yan Pan, Zhizhi Guo, Hang Zhou, Zhibin Hong, Xiaoguang Han, Junyu Han, Jingtuo Liu, Errui Ding, and Jingdong Wang. 2022. Expressive talking head generation with granular audio-visual control. In *Proceedings of the IEEE/CVF Conference on Computer Vision and Pattern Recognition*. 3387–3396.
- C.Z. Lin, D.B. Lindell, E.R. Chan, and G. Wetzstein. 2022. 3D GAN Inversion for Controllable Portrait Image Animation. In *ECCV Workshop on Learning to Generate 3D Shapes and Scenes*.
- Zhiyuan Ma, Xiangyu Zhu, Guo-Jun Qi, Zhen Lei, and Lei Zhang. 2023. OTAvatar: One-shot Talking Face Avatar with Controllable Tri-plane Rendering. In *Proceedings of the IEEE/CVF Conference on Computer Vision and Pattern Recognition*. 16901–16910.
- Ben Mildenhall, Pratul P Srinivasan, Matthew Tancik, Jonathan T Barron, Ravi Ramamoorthi, and Ren Ng. 2020. NeRF: Representing Scenes as Neural Radiance Fields for View Synthesis. In *Eur. Conf. Comput. Vis.*
- Songyou Peng, Michael Niemeyer, Lars Mescheder, Marc Pollefeys, and Andreas Geiger. 2020. Convolutional occupancy networks. In *Eur. Conf. Comput. Vis.*
- Yuri Ren, Ge Li, Yuanqi Chen, Thomas H Li, and Shan Liu. 2021. Pirenderer: Controllable portrait image generation via semantic neural rendering. In *Proceedings of the IEEE/CVF International Conference on Computer Vision*. 13759–13768.
- Elad Richardson, Yuval Alaluf, Or Patashnik, Yotam Nitzan, Yaniv Azar, Stav Shapiro, and Daniel Cohen-Or. 2021. Encoding in Style: a StyleGAN Encoder for Image-to-Image Translation. In *IEEE Conf. Comput. Vis. Pattern Recog.*

- Daniel Roich, Ron Mokady, Amit H Bermano, and Daniel Cohen-Or. 2021. Pivotal Tuning for Latent-based Editing of Real Images. *arXiv preprint arXiv:2106.05744* (2021).
- Vincent Sitzmann, Justus Thies, Felix Heide, Matthias Nießner, Gordon Wetzstein, and Michael Zollhöfer. 2019. DeepVoxels: Learning Persistent 3D Feature Embeddings. In *IEEE Conf. Comput. Vis. Pattern Recog.*
- Jingxiang Sun, Xuan Wang, Yichun Shi, Lizhen Wang, Jue Wang, and Yebin Liu. 2022. IDE-3D: Interactive Disentangled Editing for High-Resolution 3D-aware Portrait Synthesis. *SIGGRAPH ASIA* (2022).
- Jingxiang Sun, Xuan Wang, Lizhen Wang, Xiaoyu Li, Yong Zhang, Hongwen Zhang, and Yebin Liu. 2023. Next3d: Generative neural texture rasterization for 3d-aware head avatars. In *Proceedings of the IEEE/CVF Conference on Computer Vision and Pattern Recognition*. 20991–21002.
- Junshu Tang, Bo Zhang, Binxin Yang, Ting Zhang, Dong Chen, Lizhuang Ma, and Fang Wen. 2023. 3DFaceShop: Explicitly Controllable 3D-Aware Portrait Generation. *IEEE Transactions on Visualization and Computer Graphics* (2023).
- Ayush Tewari, Mohamed Elgharib, Gaurav Bharaj, Florian Bernard, Hans-Peter Seidel, Patrick Pérez, Michael Zollhofer, and Christian Theobalt. 2020. Stylerig: Rigging stylegan for 3d control over portrait images. In *Proceedings of the IEEE Conference on Computer Vision and Pattern Recognition (CVPR)*.
- Justus Thies, Michael Zollhöfer, and Matthias Nießner. 2019. Deferred neural rendering: Image synthesis using neural textures. *ACM Transactions on Graphics (TOG)* 38, 4 (2019), 1–12.
- Justus Thies, Michael Zollhofer, Marc Stamminger, Christian Theobalt, and Matthias Nießner. 2016. Face2face: Real-time face capture and reenactment of rgb videos. In *Proceedings of the IEEE conference on computer vision and pattern recognition*. 2387–2395.
- Omer Tov, Yuval Alaluf, Yotam Nitzan, Or Patashnik, and Daniel Cohen-Or. 2021. Designing an Encoder for StyleGAN Image Manipulation. *SIGGRAPH* (2021).
- Alex Trevithick, Matthew Chan, Michael Stengel, Eric R. Chan, Chao Liu, Zhiding Yu, Sameh Khamis, Manmohan Chandraker, Ravi Ramamoorthi, and Koki Nagano. 2023. Real-Time Radiance Fields for Single-Image Portrait View Synthesis. In *ACM Transactions on Graphics (SIGGRAPH)*.
- Lizhen Wang, Zhiyua Chen, Tao Yu, Chenguang Ma, Liang Li, and Yebin Liu. 2022a. FaceVerse: a Fine-grained and Detail-controllable 3D Face Morphable Model from a Hybrid Dataset. In *IEEE Conference on Computer Vision and Pattern Recognition (CVPR2022)*.
- Lizhen Wang, Xiaochen Zhao, Jingxiang Sun, Yuxiang Zhang, Hongwen Zhang, Tao Yu, and Yebin Liu. 2023. StyleAvatar: Real-time Photo-realistic Portrait Avatar from a Single Video. *arXiv preprint arXiv:2305.00942* (2023).
- Tengfei Wang, Yong Zhang, Yanbo Fan, Jue Wang, and Qifeng Chen. 2022b. High-Fidelity GAN Inversion for Image Attribute Editing. In *IEEE Conf. Comput. Vis. Pattern Recog.*
- Ting-Chun Wang, Arun Mallya, and Ming-Yu Liu. 2021b. One-shot free-view neural talking-head synthesis for video conferencing. In *Proceedings of the IEEE/CVF conference on computer vision and pattern recognition*. 10039–10049.
- Xintao Wang, Yu Li, Honglun Zhang, and Ying Shan. 2021a. Towards Real-World Blind Face Restoration with Generative Facial Prior. In *The IEEE Conference on Computer Vision and Pattern Recognition (CVPR)*.
- Yue Wu, Yu Deng, Jiaolong Yang, Fangyun Wei, Qifeng Chen, and Xin Tong. 2022. Anifacegan: Animatable 3d-aware face image generation for video avatars. *Advances in Neural Information Processing Systems* 35 (2022), 36188–36201.
- Jiaxin Xie, Hao Ouyang, Jingtian Piao, Chenyang Lei, and Qifeng Chen. 2023. High-fidelity 3D GAN Inversion by Pseudo-multi-view Optimization. In *Proceedings of the IEEE/CVF Conference on Computer Vision and Pattern Recognition*. 321–331.
- Liangbin Xie, Xintao Wang, Honglun Zhang, Chao Dong, and Ying Shan. 2022. VFHQ: A high-quality dataset and benchmark for video face super-resolution. In *Proceedings of the IEEE/CVF Conference on Computer Vision and Pattern Recognition*. 657–666.
- Hongyi Xu, Guoxian Song, Zihang Jiang, Jianfeng Zhang, Yichun Shi, Jing Liu, Wanchun Ma, Jiashi Feng, and Linjie Luo. 2023a. Omniavatar: Geometry-guided controllable 3d head synthesis. In *Proceedings of the IEEE/CVF Conference on Computer Vision and Pattern Recognition*. 12814–12824.
- Sicheng Xu, Jiaolong Yang, Dong Chen, Fang Wen, Yu Deng, Yunde Jia, and Xin Tong. 2020. Deep 3d portrait from a single image. In *Proceedings of the IEEE/CVF Conference on Computer Vision and Pattern Recognition*. 7710–7720.
- Yuelang Xu, Benwang Chen, Zhe Li, Hongwen Zhang, Lizhen Wang, Zerong Zheng, and Yebin Liu. 2024. Gaussian head avatar: Ultra high-fidelity head avatar via dynamic gaussians. In *The IEEE Conference on Computer Vision and Pattern Recognition (CVPR)*.
- Yuelang Xu, Lizhen Wang, Xiaochen Zhao, Hongwen Zhang, and Yebin Liu. 2023b. Avatarmav: Fast 3d head avatar reconstruction using motion-aware neural voxels. In *ACM SIGGRAPH 2023 Conference Proceedings*. 1–10.
- Fei Yin, Yong Zhang, Xiaodong Cun, Mingdeng Cao, Yanbo Fan, Xuan Wang, Qingyan Bai, Baoyuan Wu, Jue Wang, and Yujiu Yang. 2022. Styleheat: One-shot high-resolution editable talking face generation via pre-trained stylegan. In *European conference on computer vision*. Springer, 85–101.
- Wangbo Yu, Yanbo Fan, Yong Zhang, Xuan Wang, Fei Yin, Yunpeng Bai, Yan-Pei Cao, Ying Shan, Yang Wu, Zhongqian Sun, et al. 2023. Nofa: Nerf-based one-shot facial avatar reconstruction. In *ACM SIGGRAPH 2023 Conference Proceedings*. 1–12.
- Jingbo Zhang, Xiaoyu Li, Ziyu Wan, Can Wang, and Jing Liao. 2022. FDNerf: Few-shot Dynamic Neural Radiance Fields for Face Reconstruction and Expression Editing. *arXiv preprint arXiv:2208.05751* (2022).
- Richard Zhang, Phillip Isola, Alexei A Efros, Eli Shechtman, and Oliver Wang. 2018. The Unreasonable Effectiveness of Deep Features as a Perceptual Metric. In *IEEE Conf. Comput. Vis. Pattern Recog.*
- Xiaochen Zhao, Lizhen Wang, Jingxiang Sun, Hongwen Zhang, Jinli Suo, and Yebin Liu. 2023. Havatar: High-fidelity head avatar via facial model conditioned neural radiance field. *ACM Transactions on Graphics* 43, 1 (2023), 1–16.
- Yufeng Zheng, Victoria Fernández Abrevaya, Marcel C Bühler, Xu Chen, Michael J Black, and Otmar Hilliges. 2022. Im avatar: Implicit morphable head avatars from videos. In *Proceedings of the IEEE/CVF Conference on Computer Vision and Pattern Recognition*. 13545–13555.
- Yufeng Zheng, Wang Yifan, Gordon Wetzstein, Michael J Black, and Otmar Hilliges. 2023. Pointavatar: Deformable point-based head avatars from videos. In *Proceedings of the IEEE/CVF Conference on Computer Vision and Pattern Recognition*. 21057–21067.



Fig. 8. Qualitative comparison on the CelebA-HQ for one-shot avatar reconstruction. The results demonstrate the superior performance of our method in terms of realistic appearance recovery and fine-grained expression control.

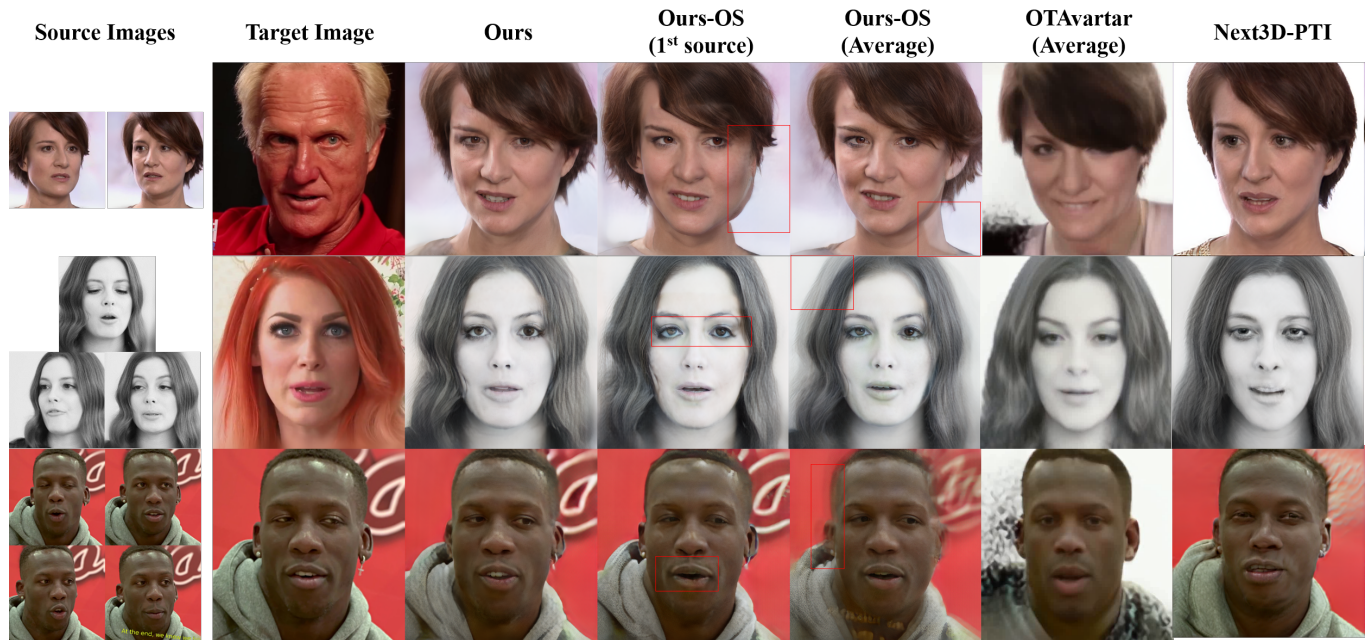


Fig. 9. Qualitative comparison on the VFHQ-Test for few-shot avatar reconstruction and animation. Our method integrates multi-frame observations to improve shape reconstruction and texture recovery, as well as retaining high fidelity. Though Ours-OS can also achieve photo-realism, it only uses the first image, and it may sometimes learn an inaccurate appearance for unobserved areas.

A IMPLEMENTATION DETAILS

In this section, we'll discuss the implementation details of each framework component, including training specifics and network architectures.

A.1 Animatable 3D GAN

We implement our 3D GAN framework on top of the official PyTorch implementation of Next3D [Sun et al. 2023], and we illustrate the differences in network architecture between ours and Next3D in Fig. 10. Next3D transforms neural texture into orthogonal views and forms tri-plane features. To compensate for the FLAME model's missing inner mouth area, Next3D utilizes a UNet G_{teeth} to supplement and reintegrate this texture, using another UNet $G_{blending}$ for post-blending. These operations are redundant and lead to heavy parameter size, so we alternately propose a more compact architecture, maintaining the insight of completing inner mouth feature conditioning on global information, but removing heavy networks for specific mouth synthesis. Specifically, we propose a face synthesis module G_{face} which is conditioned on the multi-scale rasterized neural textures. We illustrate its network architecture in Fig. 11. The multi-scale neural textures are rasterized from texture space into tri-plane space and then integrated with G_{face} 's corresponding feature maps through alpha blending. Conditioned on such global information, G_{face} is precisely controlled by the deformable mesh model, and gradually inpaint inner mouth features in the forward pass layer by layer. Additionally, our more memory-efficient and compact model design allows for neural rendering resolution of 128^2 , significantly enhancing view-consistency. Specifically, we rasterize neural texture feature maps at the resolutions of $(32, 64, 128)$ for multi-scale conditions on G_{face} .

A.1.1 Training Details. We adopt many hyperparameters and training strategies of EG3D [Chan et al. 2022] and Next3D [Sun et al. 2023] including blurred real images at the beginning, pose conditioned generator, density regularization, learning rates, and two-stage training. As for the deformation-aware discriminator, we replace the input synthetic rendering image with the landmarks counter map to force the generator to focus on the expression changes in the mouth and eyes region. During the training process, we follow Next3D and adopt the same loss terms. Specifically, we train the network on FFHQ [Karras et al. 2020], using the non-saturating GAN loss with R1 regularization and the density regularization proposed in EG3D. Based on the pretrained model of EG3D, we train our model at a neural rendering resolution of 64 on four 3090 GPUs with a batch size of 16 for roughly 2 days and gradually step the resolution up to 128 for additional 2 days.

A.2 Training Encoders

To promote inversion performance and minimize GPU memory usage during training, we adopt a three-stage training schedule, which separately trains the latent encoder E_{latent} , image encoders E_{tex} and E_{tri} in a one-shot setting, and temporal aggregation encoders E_{tex_rec} and E_{tri_rec} in a multi-shot setting.

A.2.1 Training E_{latent} . For training the latent encoder E_{latent} , we employ pixel-wise L_1 loss, perceptual loss L_{lpips} [Zhang et al. 2018],

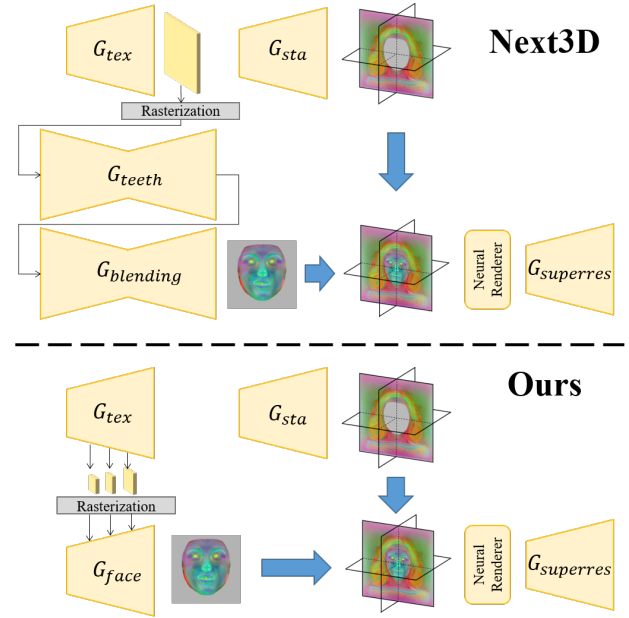


Fig. 10. Comparison of the network architecture of Next3D against ours. Our more memory-friendly and compact representation allows for efficient training at a neural rendering resolution of 128^2 , which significantly improves view consistency.

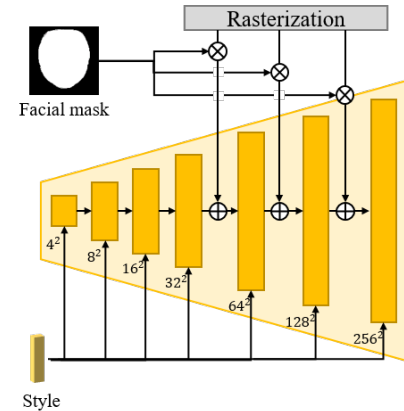


Fig. 11. The detailed architecture of G_{face} .

and identity similarity loss L_{ID} [Deng et al. 2019]. Besides, we follow [Tov et al. 2021] and set a latent discriminator D_W to discriminate between real samples from the W space and the latent codes predicted by the encoder. The encoder is trained in an adversarial scheme and the total loss can be written as :

$$L_{stage1} = L_1 + \lambda_{lpips} L_{lpips} + \lambda_{id} L_{ID} + L_{adv}^{D_W} + L_{adv}^{E_{latent}} \quad (2)$$

where $\lambda_{lpips} = 0.5$, $\lambda_{id} = 0.25$. The learning rates for the encoder and latent discriminator are both $1e-4$. Based on the FFHQ dataset, the training is conducted on four 3090 GPUs with a batch size of 16 for 2 days.

A.2.2 Training E_{tri} and E_{tex} . In this stage, we fix the latent encoder E_{latent} and train both UNet-style networks E_{tri} and E_{tex} with image datasets. Besides the FFHQ dataset, we also utilize the synthetic data generated by the pretrained GAN to prompt multi-view consistent reconstruction.

Inspired by [Trevithick et al. 2023], leveraging synthetic data, we supervise the training with intermediate feature maps, including neural texture maps F_{tex} , tri-plane feature maps F_{tri} and neural rendering feature maps I_{raw} . Loss can be written as:

$$L_{stage2} = L_1 + \lambda_{l_{pips}} L_{l_{pips}} + \lambda_{tri} L_{tri} + \lambda_{tex} L_{tex} + \lambda_{raw} L_{raw} + \lambda_{adv} L_{adv} \quad (3)$$

where $\lambda_{l_{pips}} = 1.0$, $\lambda_{tri} = 0.001$, $\lambda_{tex} = 0.001$, $\lambda_{raw} = 1.0$, $\lambda_{adv} = 0.1$. L_{tri} , L_{tex} , L_{raw} are the L1 losses that intuitively compare those quantities synthesized by our generative model and those created by our encoders. L_{adv} is the adversarial loss using a dual discriminator [Chan et al. 2022], which is trained to differentiate between synthetic images sampled from GAN prior and the corresponding image reconstructed by the encoders. We remove the pose condition for the dual discriminator. On four 3090 GPUs with a batch size of 16, we first train both image encoders without the generative adversarial objective for about 4 days, and then add adversarial loss to finetune encoders for an additional day. We use a learning rate of $1e-4$ for encoders and $1e-3$ for the discriminator.

A.2.3 Training E_{tri_rec} and E_{tex_rec} . Building upon pretrained E_{tri} and E_{tex} , E_{tri_rec} and E_{tex_rec} maintain fixed encoding backbone and only finetune their recurrent decoders. To learn to aggregate temporal information from monocular videos, we leverage 7500 real-world video clips from the VFHQ video dataset [Xie et al. 2022], each comprising 100 frames. However, since the image quality in the video dataset typically lags behind that of the GAN prior from the FFHQ dataset, training only with the VFHQ data causes blurry and degraded renderings. Hence during training, we simultaneously use the synthetic video data, which has random identity sampled from the GAN latent space, with poses and expressions sampled from the VFHQ video dataset. This additional synthetic data supplementation improves the quality of the generated images.

Due to GPU memory constraints, during training, the temporal aggregation networks E_{tri_rec} and E_{tex_rec} process a maximum of 4 frames at a time in the forward pass. This limitation can lead to overfitting on short sequences, hindering the efficient fusion of observations from longer sequences. Leveraging the RNN framework’s support for sequential inputs, we can initialize h_0 (Eq.1 in the main paper) to a non-zero state by cycling through the inputs during training. In practice, we input sequences of up to 32 frames⁵, randomly selecting 4 frames for rendering and loss calculation in each iteration. This strategy simulates the supervision over longer sequences to some extent, enhancing the ability of the update gates in GRU blocks to capture long-term dependencies and allowing the temporal aggregation networks to retain long-term temporal information.

We adopt the same loss terms and training strategy as in Sec A.2.2. On eight 3090 GPUs with a batch size of 8, we train both encoders

⁵Longer input is allowed. But for 100-frame video clips in our training data, it’s dense enough to sample 32 frames

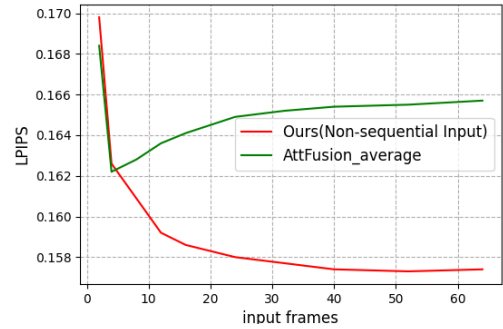


Fig. 12. LPIPS over the number of input frames on VFHQ-test. We demonstrate the effectiveness of our method to handle unordered input. Besides, we conduct a comparison with an Attention-model baseline to validate our choice of recurrent network.

without the adversarial objective for about 3 days, and then finetune with adversarial loss for additional 24 hours.

A.3 Network Architecture

Latent Encoder. To implement the latent encoder E_{latent} , we adopt the design of the e4e encoder [Tov et al. 2021] and employ IR-SE-50 [Deng et al. 2019] pretrained model for the backbone network.

One-shot Image Encoders. Adopting conventional U-Net architecture, E_{tri} and E_{tex} are designed based on TriplaneNet [Bhattarai et al. 2023]. As both networks produce multi-resolution feature maps, we incorporate an extra MLP block at each layer to transform the output channels.

Temporal Aggregation Networks. E_{tex_rec} and E_{tri_rec} are modified based on E_{tex} and E_{tri} . Specifically, we fix the down-sampling encoding part of the networks and replace the decoding parts with recurrent decoders by injecting a ConvGRU block at each layer.

B MORE EXPERIMENTS

B.1 Reason for the choice of Recurrent Network

We choose RNN for two reasons. Firstly, for few-shot tasks, the length of the input image sequence usually does not exceed 50, and GRU can handle such short sequences without suffering from forgetting issues. Secondly, despite Attention’s widespread use for unordered sequences, its high computational cost limits supported sequence lengths during training. In contrast, GRU’s computation grows linearly with sequence length, allowing the utilization of more frames for learning long-term temporal aggregation during training.

To evaluate our recurrent mechanism, we establish a fixed-window baseline termed “AttFusion”, which replaces each GRU block with a transformer block to merge temporal features. As we can only train it with 3 frames in our practice, during inference “AttFusion” averages the inverted canonical features when handling longer sequences.

To demonstrate our ability to handle non-sequential input, we randomly sample from a video to form input sequences. It can be

	FID↓	AKD↓	CSIM↑	Params
Ours	4.1	0.057	0.853	84.21M
Next3D (FV)	3.9	0.095	0.852	164.81M

Table 5. Quantitative comparison with Next3D (FaceVerse) on image synthesis quality, animation accuracy, identity preservation and memory consumption.

observed that the two curves representing our method in Fig. 12 and Fig. 6 almost overlap, indicating that our approach is comparably effective in handling both ordered and unordered data.

As illustrated in Fig. 12, Our ConvGRU-based implementation and Attention models have similar performance for short sequences. However, for longer sequences, the performance of the Attention baseline suffers from the blur caused by the averaging strategy, and our recurrent framework’s performance improves incrementally

with additional frames. Hence, we think ConvGRU is more suitable for our flexible few-shot task.

B.2 Ablation on the network design of Animatable 3D GAN

As mentioned in Sec. 3.2 and Sec. A.1, we replace the two UNets in Next3D with a single generator G_{face} . To evaluate the impact of the replacement, we use the FFHQ dataset to train Next3D network with the same facial parametric model (FaceVerse), and illustrate the quantitative comparison in Tab. 5.

Despite a slight increase in FID score due to fewer parameters, the improvement in AKD score demonstrates that our generator has more precise expression-driving performance. This is attributed to G_{face} ’s multi-scale conditioning, which enables the conditional parametric model to directly control generated facial features. In contrast, the two cascaded post-processing UNets diminish control sensitivity.

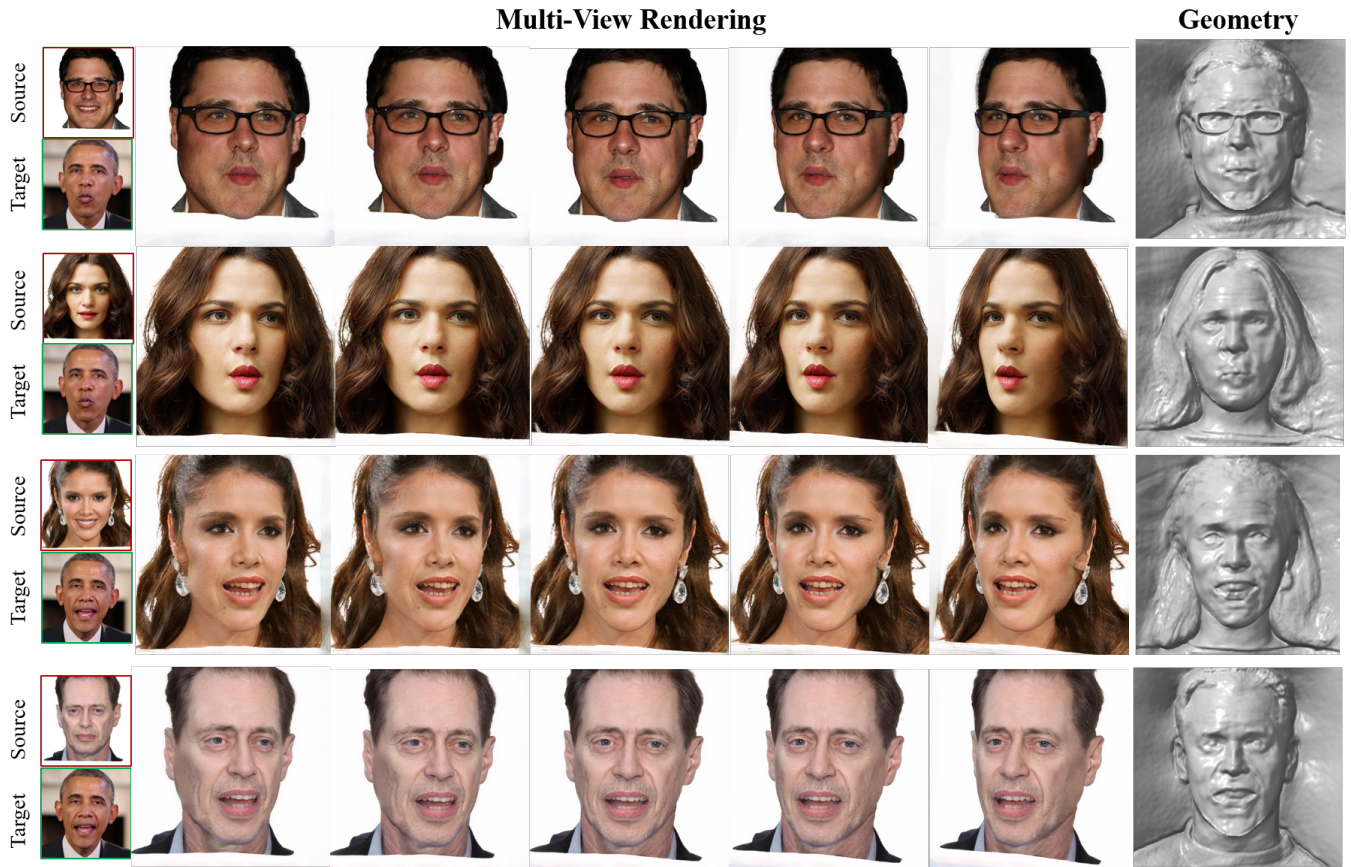


Fig. 13. Cross-identity reenactment results of one-shot avatar reconstruction. We illustrate the multi-view rendering results and geometry.